Applied Clay Science xxx (2016) xxx–xxx

Contents lists available at ScienceDirect

Applied Clay Science

journal homepage: www.elsevier.com/locate/clay

Potentials of fabricating porous ceramic bodies from kaolin for catalytic substrate applications

David O. Obada [a,*], David Dodoo-Arhin [b], Muhammad Dauda [a], Fatai O. Anafi [a], Abdulkarim S. Ahmed [c], Olusegun A. Ajayi [c,d]

[a] Department of Mechanical Engineering, Ahmadu Bello University, Zaria, Nigeria
[b] Department of Materials Science and Engineering, University of Ghana, Legon, Ghana
[c] Department of Chemical Engineering, Ahmadu Bello University, Zaria, Nigeria
[d] Department of Chemical and Petroleum Engineering, Afe Babalola University, Ado-Ekiti, Nigeria

ARTICLE INFO

Article history:
Received 9 January 2016
Received in revised form 3 June 2016
Accepted 7 June 2016
Available online xxxx

Keywords:
Kaolin
Porosity
Physical properties
Pore formers
Green bodies

ABSTRACT

In this work, the suitability of using kaolin–styrofoam, sawdust, and high density polyethylene to produce porous ceramic bodies was experimentally investigated. The kaolin samples (raw and beneficiated) were characterized by the XRD, SEM, TGA/DSC and FTIR methods. Batch formulations of the samples including the kaolin and pore formers were formed into green bodies and fired to 1150 °C. The porosities of sintered bodies were calculated and gave the following: apparent porosity: 28.63%–67.13% for all the samples investigated. Samples with high density polyethylene (HDPE) pore formers showed minor surface cracks after firing, but exhibited the highest porosity levels while samples with styrofoam and saw dust exhibited uniform surface characteristics with pores, thermal stability and no visible surface cracks. It can be concluded that formulations containing 80% kaolin can be used for the production of ceramics with porosities as high as 67% if the right pore formers are used.

1. Introduction

The presence of porosity in materials for industrial applications is often viewed as problematic. However, there are many applications in which the use of porous materials can be advantageous or even necessary, for example in filters, membranes, catalytic substrates, thermal insulation, gas burner media, and as refractory materials. Generally, porous ceramics are usually understood as materials having porosity levels which are over 30% (Guzman, 2003). They could be considered as systems that consist of a solid substance that forms walls between pores (a skeleton) and air that normally fills the pores. The composition, pore characteristics, and crystal structure are the main parameters determining the thermo-physical properties of porous ceramics (Ulyanova et al., 2006). Various processing routes/methods have been applied in manufacturing porous ceramics and they have recently been reviewed by Studart et al. (2006). These methods include but not limited to replica, sacrificial template and direct foaming methods while many other techniques are being developed, where a change of a host of parameters leads to different types of product from the same starting materials. The development of porous ceramics is attractive because porous ceramics are more stable in severe environments and they can be engineered to satisfy specific requirements due to their surface characteristics. Various porous media such as metal foams (Dukhan, 2012), wood (Kim and Pal, 2010), porous polymers (Liu et al., 2014), porous nano-composites (Li et al., 2012) and ceramic foams (Colombo, 2002) have been used for a variety of industrial applications in battery electrodes, vehicular furnishing, catalytic converters, etc. Amongst the porous materials, there has been an increasing demand for porous ceramics in industrial applications due to their high temperature stability and the ability to tailor their pore sizes for specific operations. (Efavi et al., 2012; Hammel et al., 2014).

Porous ceramic bodies are usually made from aluminosilicates and several technologies are available for their fabrication (Chen et al., 1998; Sandford and Sibley, 1996). The nature of raw materials used in the various fabrication routes however affects the porosity (pore size), surface, chemical inertness and also the thermal shock resistance of porous ceramic bodies (Taslicukur et al., 2007).

Kaolinite has gained a lot of research interest due to its relative simplicity both structurally and chemically. Though it usually contains a variety of structural defects, the structural orderliness of these kaolinites tend to influence many of the properties which are exploited industrially. Kaolinite and more specifically ordered kaolinite have been found to be of immense application in alum and alumina production (Al-Zahrani and Abdel-Majid, 2004; Hosseini et al., 2011), ceramics, zeolite catalysts, catalyst supports for auto-exhaust purification, adsorbents for heavy

* Corresponding author.
E-mail address: obadavid4@gmail.com (D.O. Obada).

http://dx.doi.org/10.1016/j.clay.2016.06.006
0169-1317/

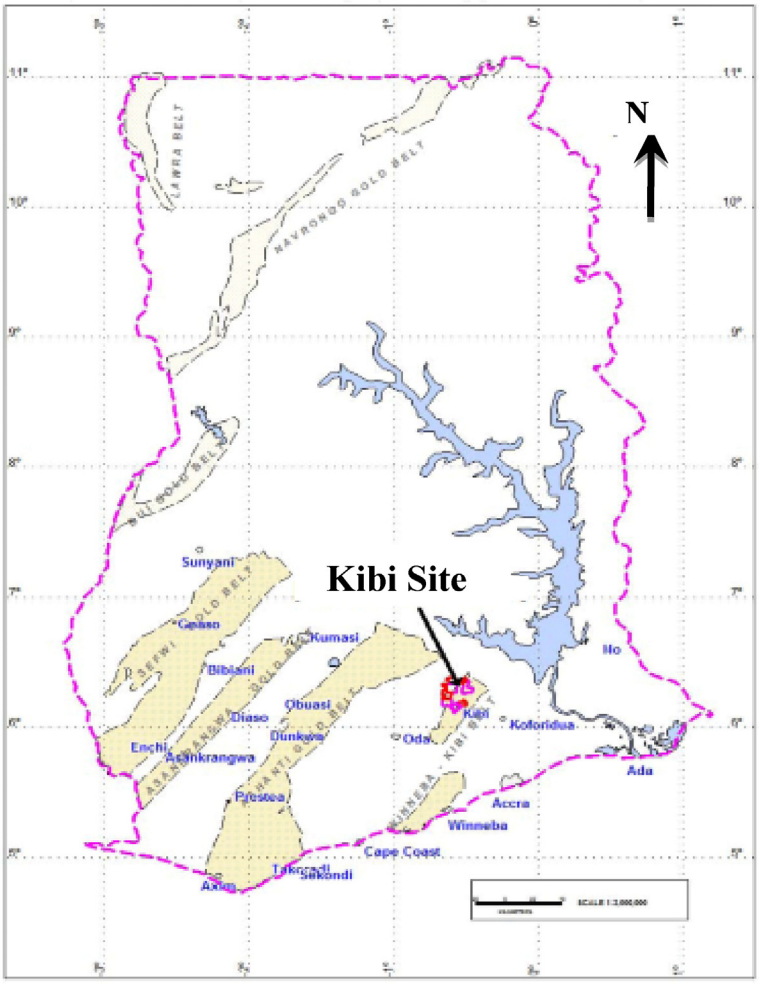

(a)

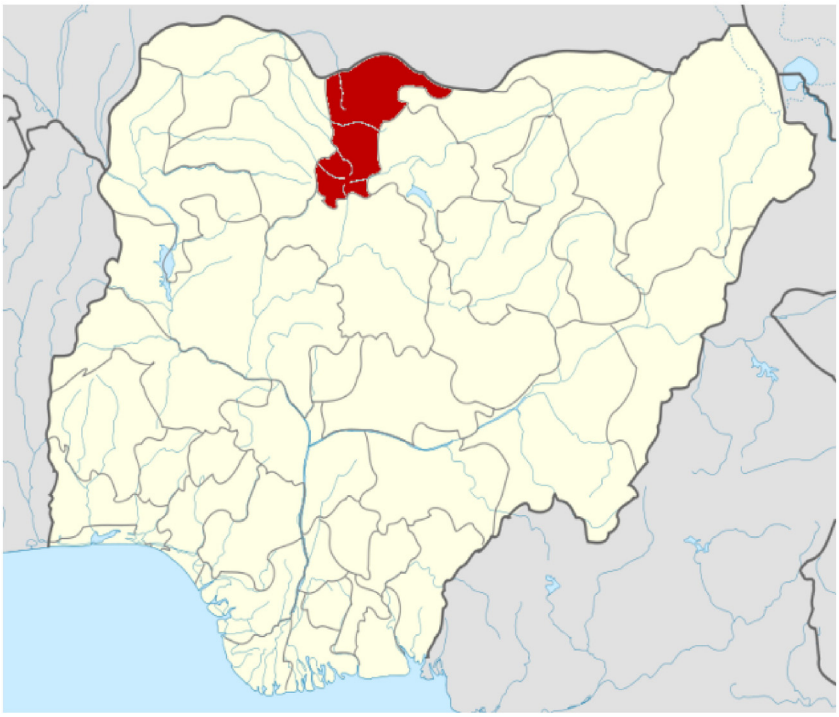

(b)

Fig. 1. Map of (a) Kibi, Eastern region of Ghana and (b) Kankara, Katsina Region of Nigeria.

Please cite this article as: Obada, D.O., et al., Potentials of fabricating porous ceramic bodies from kaolin for catalytic substrate applications, Appl. Clay Sci. (2016), http://dx.doi.org/10.1016/j.clay.2016.06.006

Table 1
Composition of Batch formulation (Total weight = 100 g).

Sample code.	Kaolin (g)	Plasticizer (Kibi Kaolin) (g)	Saw dust (g)	Styrofoam	High density polyethylene (HDPE)
A	70	20	10	–	–
B	60	20	20	–	–
C	70	20	–	10	–
D	60	20	–	20	–
E	70	20	–	–	10
F	60	20	–	–	20
G	80	20	–	–	–

metals and currently in catalysis, to mention a few (Murray, 2000, 2007; Bergaya et al., 2006; Murray and Kogel, 2005; Churchman et al., 2006; Adams and McCabe, 2006).

Properties of kaolinite, particularly important for industrial applications are particle-size distribution, structural order-disorder or crystallinity, surface area and whiteness (Murray, 2000). The order degree of kaolinites strongly influences their physical and chemical properties. The most often used method for examination of the degree of structural disorder or "crystallinity" of the kaolinite samples is X-ray powder diffraction. The XRD patterns of ordered kaolinite samples are significantly different from those of disorder. Ordered kaolinite shows sharp and narrow peaks, while its disordered counterpart gives less well-defined, broad, and asymmetrical peaks (Brigatti et al., 2006). The crystallinity indices given by many authors are widely used for determination of kaolinite disorder degree using various approaches based on X-ray diffraction (Brindley et al., 1963; Plancon and Zacharie, 1990; Aparicio and Galán, 1999; Chmielová and Weiss, 2002; Aparicio et al., 2006). Also it has been observed that less common method used for determination of kaolinite disorder degree is infrared spectroscopy. The structural disorder of kaolinites can be detected by differences in position and relative intensity of OH stretching and bending bands in IR spectrum (Madejová and Komadel, 2001; Muller and Bocquier, 1987; Prost et al., 1989).

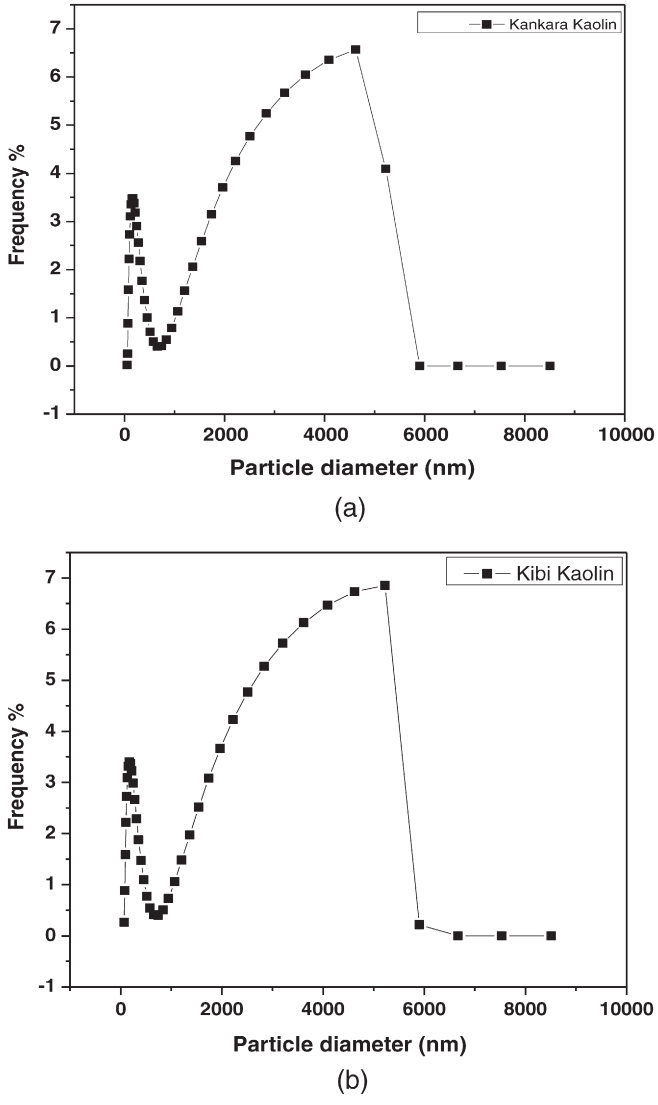

Fig. 2. Particle size distribution of Kankara and Kibi Kaolin.

Numerous pore-forming agents have been investigated, including starch (Zivcová et al., 2012; Khattab et al., 2012; Garrido et al., 2011; Chen et al., 2011; Zivcová et al., 2009; Zivcová et al., 2010; Gregorová et al., 2006), graphite (Sarikaya and Dogan, 2013; Sanson et al., 2008; Ding et al., 2007; Boaro et al., 2003), lycopodium (Zivcová et al., 2007; Zivcová et al., 2008; Seržane et al., 2010), sucrose (Sarikaya and Dogan, 2013: Ray et al., 2010; Wang et al., 2005) and polymethyl methacrylate (Zeng et al., 2007; Yao et al., 2005; Kumar et al., 2005) and others (Bai et al., 2012; Horri et al., 2012 and Silva et al., 2002). Even though starch is the most frequently used pore forming agent, possibly due to its biological origin and availability, the difficulties in maintaining the pore structure formed by the starch burn out, and the narrow size range of commercially available starch types (typically between 5 and 50 μm) limits its application when large pores are desirable (Gregorová and Pabst, 2007).

As stated, a lot of pore-forming agents have been investigated, however, to the best of our knowledge, no report regarding the use of powdery high density polyethylene (PHDPE) has been reported so far for its potential in creating voids in a ceramic body after solid state sintering. Hence, this experimental investigation therefore aims to develop ceramic bodies from kaolin deposits sampled from Kankara and Kibi regions in Katsina-Nigeria and Kibi-Ghana using sawdust, high density polyethylene and styrofoam as pore formers.

2. Experimental methods

2.1. Raw material beneficiation and powder preparation

The two kaolin samples used were mined from deposits at Kankara in Katsina State of Nigeria and Kibi in the Eastern region of Ghana as shown in Fig. 1.

The raw mined kaolin samples were washed off their impurities by adding water to a constantly stirred kaolin blunger to obtain slurry with specific gravity of about 1.2. The slurry was then passed through a 350 μm sieve to eliminate coarse grained impurities; poured into a Plaster of Paris mold (POP) and the filtrate dried in an oven at a temperature of 120 °C for 7 h. The essential properties of the raw material such as particle size ranges were experimentally determined. A laser method, low-angle laser light scattering (LALLS), was used for the particle size analysis with levels of sensitivity in the 0.3 nm to 8 μm range using a Horiba Scientific, SZ-100 nanoparticle analyzer. 10 mg of the kaolin samples (Kankara and Kibi) plus freshly deionized water (10 mg of

Please cite this article as: Obada, D.O., et al., Potentials of fabricating porous ceramic bodies from kaolin for catalytic substrate applications, Appl. Clay Sci. (2016), http://dx.doi.org/10.1016/j.clay.2016.06.006

Table 2
Chemical compositions of the Kankara and Kibi kaolin.

Component	SiO_2	Al_2O_3	Fe_2O_3	TiO_2	MgO	CaO	Na_2O	K_2O	CuO	LOI*
KKR fraction (wt%)	54.30	28.32	0.84	0.10	0.44	1.90	0.22	3.94	0.02	9.77
KKB fraction (wt%)	51.50	28.20	0.91	0.12	0.47	1.21	0.61	1.80	0.02	15.01
KBB fraction (wt%)	45.81	39.24	0.95	1.46	ND	0.01	0.02	0.84	0.01	11.09

LoI* = Loss on ignition, KKR = Raw Kankara Kaolin; KKB = Beneficiated Kankara Kaolin; KBB = Beneficiated Kibi Kaolin.

kaolinite + 10 mL of water) were subjected to continuous ultrasound treatment in an ultrasonic bath for 15mins to ensure dilution and homogenous dispersion. The pore formers comprising saw dust, styrofoam and high density polyethylene were prepared using an analytical mill to reduce the sizes.

2.2. X-ray fluorescence (XRF)

The chemical compositions of the samples were determined using a Panalytical Minipal 4 X-ray fluorescence analyzer equipped with Omnium software for analysis. The samples were milled to achieve particle sizes <75 μm, dried at 100 °C and roasted at 1000 °C to determine Loss on Ignition (LOI) values. About 1 g of each sample was mixed with 6 g lithium tetraborate flux ($Li_2B_4O_7$) and fused at 1050 °C to obtain a stable fused glass bead. For trace elemental analyses, the sample was mixed with a PVA binder and pressed into a pellet.

2.3. XRD analysis and crystallinity index

To determine the crystalline domain size, phases present, and the kaolinite order X-ray powder diffraction (XRD) patterns were collected on an Empyrean diffractometer (Panalytical BV, Netherlands) with theta/theta geometry, operating Cu Kα radiation tube (λ = 1.5418 Å) at 40 kV and 45 mA. The XRD patterns of all the randomly oriented powder specimens were recorded in the 5.0°–70° 2θ range with a step size of 0.017° and a counting time of 14 s per step. The diffraction patterns were matched against the ICSD's PDF database and qualitative phase analysis conducted using the X'Pert Highscore plus search match software (Panalytical, The Netherlands). The order of the kaolinite samples was determined using the Hinckley index (HI) (Hinckley, 1963). The estimated average crystallite sizes of the kaolinite samples were also calculated from the X-ray diffraction pattern by using the Scherrer broadening method based on the basal 002 reflection with peak position at (26.8°, 2θ) and the 001 plane at 12.8°, 2θ (Scherrer, 1918). The Scherrer equation is given as $\beta(2\theta) = \frac{K\lambda}{L\cos\theta}$ where K is the Scherrer constant for shape factor vales, λ is the wavelength of the radiation source, θ is half of the diffraction angle, β is the peak width (Full width at Half Maximum-FWHM) and L is the crystallite size.

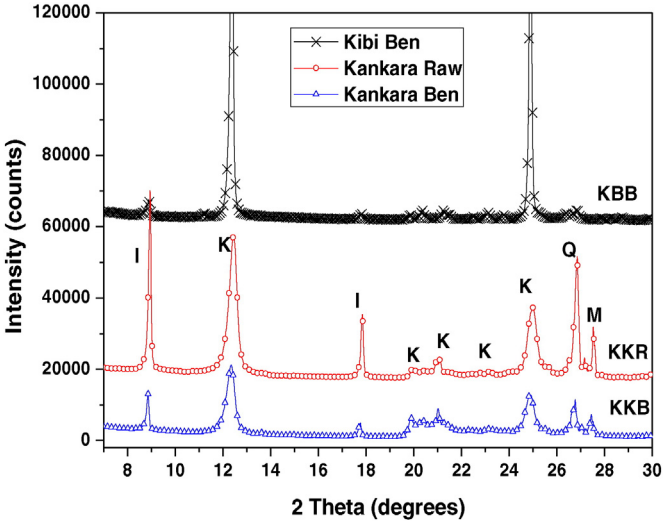

Fig. 3. XRD patterns of raw Kankara kaolin, beneficiated Kankara kaolin and Kibi kaolin. Kaolinite (K), Illite (I), Muscovite (M) and Quartz (Q).

2.4. Fourier infrared spectroscopy

To further probe the structure, quality and figure prints of the kaolinite samples, Attenuated Total Reflectance (ATR) Fourier Transform Mid Infra-Red spectra were recorded on a HYPERION 3000 (Bruker Optics) instrument in the 4000–400 cm^{-1} range with a resolution of 2 cm^{-1}. The powder samples were measured without the addition of KBr. Sample compartment was evacuated during acquisition and the contact between the sample and the Attenuated Total Reflectance (ATR) diamond crystal was 2 mm diameter.

2.5. Thermogravimetry

The thermal stability of the various phases in the samples was studied by DTA/TG under air flow of 50 mL/min. The samples were thermally analysed by placing ≈25 mg of the specimens in an alumina (Al_2O_3) crucible (100 mg capacity), subjected to a linear heating ramp between 100 °C and 700 °C at a rate of 10 °C/min and a cooling rate of 50 °C/min, in NETZSCH, STA 449C Jupiter TG/DSC instrument. The test measurements were made for the mass change (loss) of the sample as a function of the temperature and the phase changes by the adsorption or the emission of energy.

2.6. Scanning electron microscopy

Scanning electron microscopy analysis was conducted to study the morphological features of the various layers of the kaolinite samples using an ultra-high vacuum and high resolution FEI,Xl-30 scanning electron microscope. Samples were metalized with gold/platinum coating prior to the analysis. Images were acquired at magnifications of 8000× and 15,000× and 10,000× for kaolinites and at 500× for sintered samples.

2.7. Formation of porous green bodies

Different sets of batch formulated samples composed of Kankara and Kibi kaolin and pore formers (sawdust, high density polyethylene and styrofoam) were mixed with water and kneaded to eliminate lumps, trapped air bubbles and to ensure homogeneity. (see Table 1 for detailed compositions of samples). The sample without pore former has been used as a control sample. The samples have been coded A, B, C, D, E, F and G. A and B are ceramic bodies with 10 and 20 wt% of sawdust as pore former, C and D are ceramic bodies with 10 and 20 wt% of styrofoam as pore former E and F are ceramic bodies with 10 and 20 wt% of HDPE as pore former while G is the control sample with no pore former (100% kaolin).

Since Kibi kaolin was experimentally observed to be more plastic, it was used mainly as a plasticizer in the batch formulations. The kaolin-pore former mixture was then completely filled into a mold and pressed to the same level to ensure compactness and dimensional homogeneity.

Please cite this article as: Obada, D.O., et al., Potentials of fabricating porous ceramic bodies from kaolin for catalytic substrate applications, Appl. Clay Sci. (2016), http://dx.doi.org/10.1016/j.clay.2016.06.006

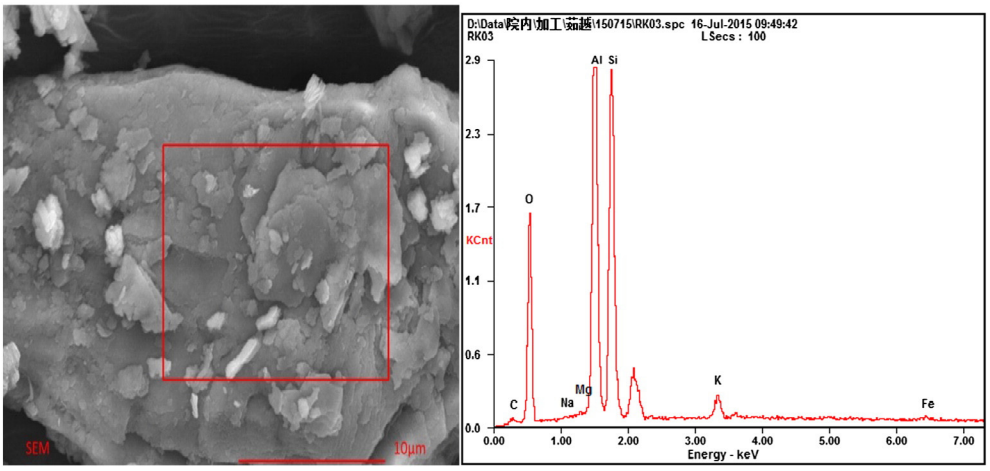

Fig. 4. SEM and EDS of raw Kankara kaolin.

The as-prepared green body samples were removed from the mold and dried at room temperature (ca. 25 °C) on boards for three (3) days after which they were further dried at 100 °C to remove moisture. This increased their green strength and made them safe for subsequent handling. The dried batch-formulated green bodies were then sintered at 1150 °C for 2 h in an electric muffle furnace at a heating rate of 5 °C/min. The apparent porosity (the amount of void or pores within a volume of porous solid) of the as-sintered kaolin based ceramic bodies was calculated using Eq. .(1):

$$\text{Apparent porosity} = \left(\frac{W-D}{W-S}\right) \times 100 \quad (1)$$

where: W = Weight of soaked specimen suspended in air; D = Weight of fired specimen and S = Weight of fired specimen suspended in water.

3. Results and discussion

3.1. Sieve size analysis

The particle size distribution of the kaolin samples (Kankara and Kibi) after particle size analysis is shown in Fig. 2. There is a broad range of particle sizes in the samples (<1 nm–8000 nm) which is necessary for close packing configuration (Kingery et al., 1976; Richerson, 2006).

Table 2 presents the chemical analysis of the raw Kankara kaolin and beneficiated Kankara and Kibi kaolin. There was no appreciable reduction in MgO, CuO and TiO for the Kankara kaolin. MgO was also not detected in the Kibi Kaolin. Nevertheless, some appreciable reductions were observed in the K_2O and CaO after beneficiation for the Kankara and Kibi Kaolin. For the Kankara kaolin which is the base material, K_2O reduced by 54.3% while CaO reduced by 36.31%. The reductions observed vis-à-vis raw kaolin generally, likely occurred as a result of washing off of soluble salts of potassium and calcium during the beneficiation process. It is worth noting that Na_2O and Fe_2O_3 had rather increased for the Kankara Kaolin after the beneficiation. It was not clear what was responsible for the increment, however, the same trend have been reported for Kankara clay by other researchers (Edomwonyi-Otu, et al., 2013). The LOI of the raw Kankara kaolin was 9.77 wt%, it increased by 34.9% after beneficiation. The increase after beneficiation could be attributed to increase in clay content of the kaolin resulting from washing away of impurities.

3.2. XRD patterns and Hinckley index of kaolinite

Fig. 3 presents the XRD pattern of the raw and beneficiated Kankara kaolin (KKR and KKB) in addition to beneficiated Kibi kaolin (KBB). The raw material is composed of kaolinite, quartz and montmorillonite. (See Figs. 4 and 5.)

The beneficiated kaolin is mainly composed of kaolinite. The reduction in the intensity of the quartz could be attributed to reduction in the concentration due to washing away during the beneficiation process. The same can be said for the XRD pattern of KBB. The main characteristic peaks of kaolinite (12.35° and 24.88°) have also been observed. The narrow and intense peaks confirm that these kaolinites are well crystallized.

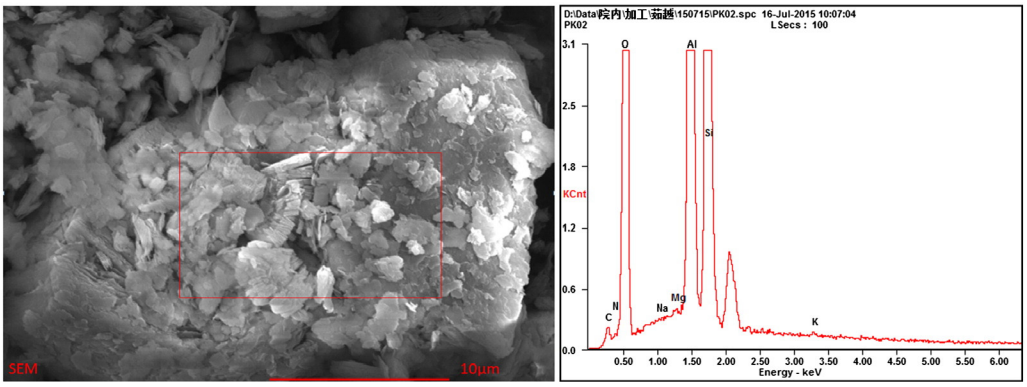

Fig. 5. SEM and EDS of beneficiated Kankara kaolin.

Please cite this article as: Obada, D.O., et al., Potentials of fabricating porous ceramic bodies from kaolin for catalytic substrate applications, Appl. Clay Sci. (2016), http://dx.doi.org/10.1016/j.clay.2016.06.006

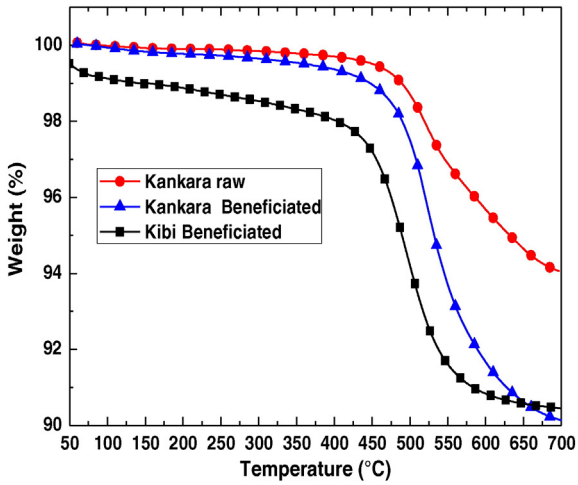

Fig. 6. Comparison of TG curves for raw and beneficiated Kankara kaolin and beneficiated Kibi kaolin.

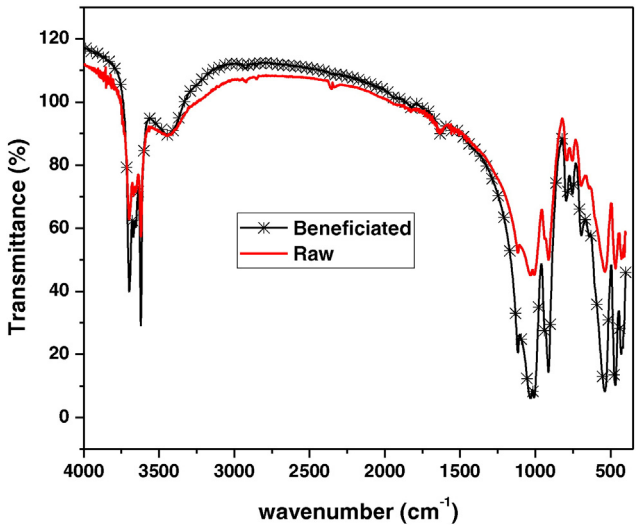

Fig. 8. Comparison of FTIR spectra of raw and beneficiated Kankara kaolin.

The Hinckley index for beneficiated Kankara kaolin was found to be 0.9199 while that of Kibi Kaolin was found to be 1.313. This indicates that the Kibi kaolin is more crystalline than the Kankara kaolin. From literature (Scherrer, 1918), the common K values include 0.89–1.0 for spherical crystals with cubic symmetry and from 0.62 to 2.08 for various crystal structures. The average crystallite sizes for Kibi kaolin are 32.109 nm (K = 0.62), 51.79 nm (K = 1), 107.724 nm (K = 2.08) and that of Kankara kaolin are 12.969 nm (k = 0.62), 20.51 nm (k = 1), 43.51 nm (k = 2.08).

3.3. SEM micrographs of Kankara and Kibi kaolin

Plates I, II, III and IV show the SEM images of the raw and beneficiated Kankara and Kibi kaolin respectively, scanned at various magnifications. The platelet morphology of kaolinite clay reported in the literature (Abo-El-Enein et al., 2013; Bergaya and Lagaly, 2013) which normally portrays booklets morphology could be clearly observed. Plates I and III (A and B) show the SEM scan at magnifications of 8000 and 15,000× for the raw kaolin (Kankara and Kibi) while Plates II and IV (A and B) show the SEM scan at magnifications of 8000 and 15,000× for the beneficiated kaolin (Kankara and Kibi). Each of the images showed a booklet morphology consisting of platelet sheets of kaolinite mineral as reported in the literature. The average particle size was estimated as 2.0 μm for both the raw and beneficiated kaolin.

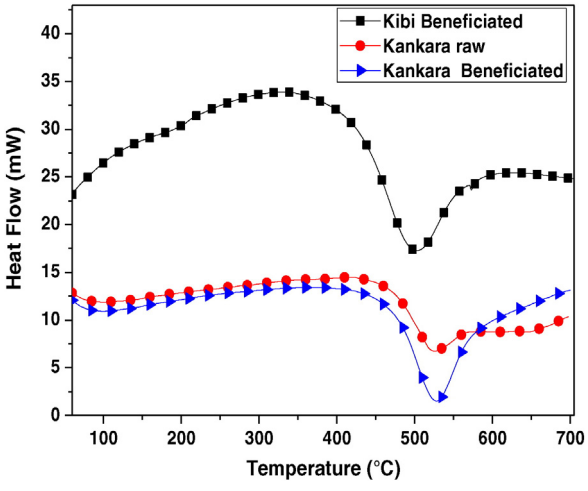

Fig. 7. Comparison of DSC curves for raw and beneficiated Kankara kaolin and beneficiated Kibi kaolin.

3.4. Thermogravimetric behaviour of kaolin samples

Figs. 6 and 7 show the TG/DSC curves of the KKR, KKB and KBB. It could be observed from Fig. 6 that the three materials have similar thermogravimetric curves. The TG curves show the weight loss associated with thermal treatment of Kankara kaolinite up to 700 °C. It can be observed that the remarkable loss occurred between 450 °C and 600 °C and stabilized at about 700 °C for beneficiated Kankara kaolin. As regards the beneficiated Kibi kaolin, it was observed that the remarkable loss occurred between 500 °C and 550 °C and stabilized around 600 °C and for the raw Kankara Kaolin, it was observed that the remarkable loss occurred between 450 °C and 600 °C and stabilized at about 700 °C. These correspond to a transformation of phase from the crystalline kaolinite to the amorphous metakaolin for all the materials. This observation is corroborated where dehydroxylation of Kankara kaolinite is seen between 500 °C and 600 °C for the kaolinite corresponding to a weight loss of about 9.4%, 8.0% and 14.8% respectively in agreement with literature expectations (Bich et al., 2009).

Both curves depicted in Figs. 6 and 7, for TGA and DSC, are of a typical shape for kaolin based materials. Since the sample was not fully dried, some physically bounded water was present at the surface defects on walls of kaolinite crystals (Polakovič et al., 1983) and in micropores, which caused a subsequent loss of the sample mass at the lowest temperatures. This is as confirmed by the endothermic peaks as shown by the DSC curve around 100 °C. From the TG curve, absorbed water is gradually evolved at temperatures up to 200 °C. The dehydroxylation reaction occurs in the temperature range of about 450°–700 °C. Experimental factors, such as the heating rate, large sample particle size and so on can shift the initial and final temperatures of the dehydroxylation, hence the slight differences in mass depletion of the three materials.

Fig. 7 shows a typical DSC plot of the three materials and offer a basis for comparison. The following peaks can be observed: desorption of water from ambient to 110 °C (Endotherm) for raw and beneficiated Kankara kaolin and dehydroxylation of the crystal lattice (450–700 °C) (Endotherm process with a T_{min} = of about 528.56 °C) for all the three materials. The phase transformation of the beneficiated kaolin at a lesser temperature to metakaolin plays a key role in the thermal stability of kaolin based ceramics during sintering.

Please cite this article as: Obada, D.O., et al., Potentials of fabricating porous ceramic bodies from kaolin for catalytic substrate applications, Appl. Clay Sci. (2016), http://dx.doi.org/10.1016/j.clay.2016.06.006

Fig. 9. Green bodies during drying at room temperature.

3.5. FTIR analysis

Fig. 8 shows the FTIR analysis of Kankara kaolin (raw and beneficiated kaolin). The absorption bands at 3698.1–3619.9 cm^{-1} and 3697.6–3620.4 cm^{-1} express the stretching vibrations of OH groups of kaolinite for raw and beneficiated kaolin respectively (Antunes et al., 2013; Galos, 2011; Gasparini et al., 2013). The bands located at 3441.1 and 1116.1 cm^{-1} and 3441.1 and 1115.9 cm^{-1} corresponds respectively to stretching vibrations of water molecules (Yusiharni and Gilkes, 2012) while those at 1031.8 cm^{-1} and 1031.9 cm^{-1} and then at 912.0 cm^{-1} and 912.7 cm^{-1} express respectively the vibrations of *Si*- O– Si and Si- O– Al groups of the network. The bands at 789.7 and at 694.9 cm^{-1}, and 796.2 and 693.0 cm^{-1} indicates the presence of the stretching vibration of Al-OH with Al in coordination for raw and beneficiated kaolin respectively. The band at 477.7 cm^{-1} and 479.6 cm^{-1} indicates the vibrations of Si-O-Si and Si-O-Al groups of the network for the raw and beneficiated kaolin respectively. In summary, the spectra exhibited OH stretching at bands 3698.1, 3619.9 3697.6 and 3620.4 cm^{-1} respectively, and the OH deformation bands were observed at 912.0 and 912.7 cm^{-1} for the raw and beneficiated samples tested respectively. Bands associated with SiO stretching were 789.7, 694.9, and 796.2 and 693.0 cm^{-1} respectively, whereas SiO deformation bands were 1031.8 and 1031.9 cm^{-1}. It is observed that the bands obtained for raw kaolinite are close to those obtained for beneficiated kaolinite.

3.6. Formation of porous green bodies

Fig. 9 shows compacted images of dried green bodies ready for firing. The green body's strength is important because a weak green body is likely to shatter in the course of sintering. After the drying period, it was observed that the samples with high percentage of pore formers (sawdust, styrofoam and high density polyethylene) either cracked or warped (twist). This observation is attributed to the nature of the pore formers used. After firing, the high density polyethylene formed samples had some surface cracks, high porosity, uneven cleavages in broken samples, not too noticeable discoloration and distorted dimension (Fig. 10). These characteristics are attributed to the nature of pore formers used. This observation indicates that the disintegration of the fired sample results from release of large volume of CO_2, H_2O vapour and other gaseous volatiles during firing.

Most of the porous ceramics did not show any significant sign of discoloration despite the release of large volumes of CO_2 from the combustible pore formers. This could be attributed to complete burn out of organic solvents and the transition of green bodies from hydrous to anhydrous states after the evaporation effect is over. This tendency is observed at higher temperatures. The samples after firing exhibited some thermal stability and compactness without indications of severe surface cracks or distortions. This is attributed to lower melting temperatures of the pore formers. It is commonly believed that the relatively large volume change accompanying the $\beta \rightarrow \alpha$ transformation of the unsolved quartz grains ($\Delta V/V = -0.68\%$ for free quartz grain) is the basic source of microcracking. After removing the weakly bound physically absorbed water, the sample loses the rest of this water and a very small amount of the organic material. The values of the thermal expansion increase up to ~500 °C when dehydroxylation occurs, which leads to a contraction of the sample and dropping of its mass. Following the escape of the physically bound water, there is no further change in the structure and composition. The temperature interval of dehydroxylation is considered a critical stage of the firing process. It is known that an inadequate high rate of heating or cooling leads to cracking of the ceramic body. This was only observed significantly on samples E and F which can also be attributed to the high porosity in the samples. Fig. 10 shows the ceramic bodies after sintering.

Fig. 11 show SEM images of control sample and samples with 10 wt% of pore formers fired at 1150 °C for a holding time of 2 h. It was seen that both macropores and micropores were interconnected. From images A–C some cracking or intervening pore walls were also seen due to the fraction of pore formers embedded (10 wt%). It can be observed that images A–C show the porosities that have been embedded into the samples by virtue of the combustible pore formers (large dark holes in the images), while image D, by reason of experimentation showed some visible pores not comparable to the others, and obviously had very limited pores embedded. This is in line with results obtained for apparent porosity (see Table 3), where it was noted that materials with porosity levels less than 30% cannot be said to be porous.

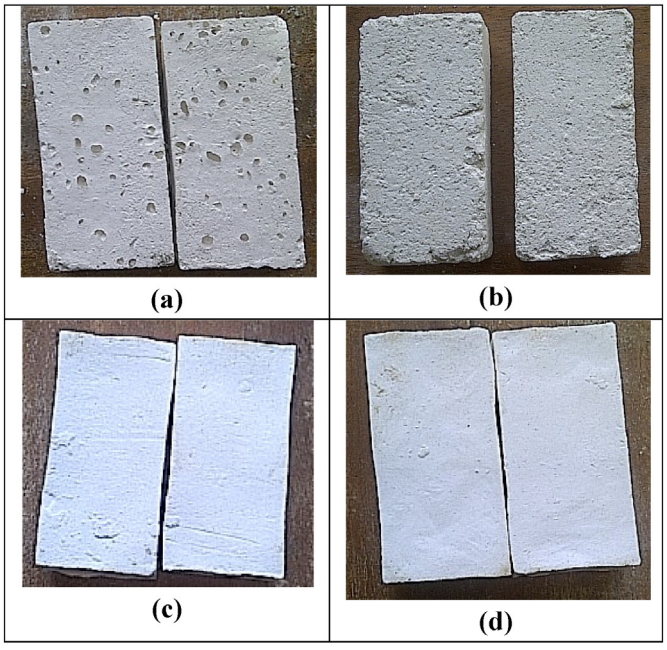

Fig. 10. Sintered bodies at 1150 °C. a) Sample with styrofoam b) Sample with PHDPE c) Sample with sawdust d) Sample without pore formers.

Please cite this article as: Obada, D.O., et al., Potentials of fabricating porous ceramic bodies from kaolin for catalytic substrate applications, Appl. Clay Sci. (2016), http://dx.doi.org/10.1016/j.clay.2016.06.006

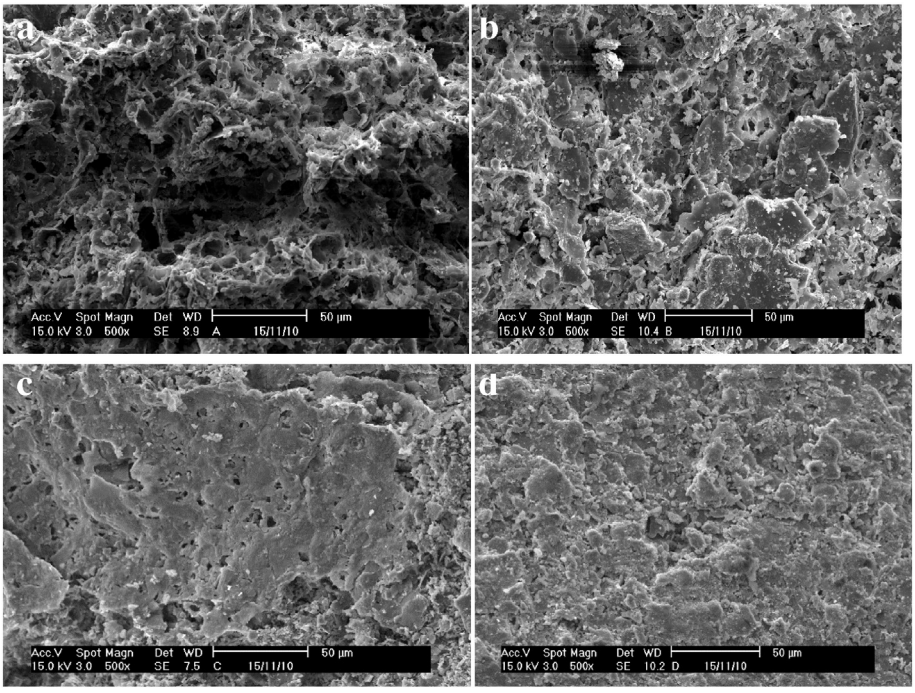

Fig. 11. SEM images of sintered samples: A) Sample with Styrofoam B) Sample with high density polyethylene C) Sample with sawdust D) Sample without pore formers.

Generally, porous ceramics are usually understood as materials having porosity over 30% (Guzman, 2003). The apparent porosity of the ceramic bodies increased with increasing amount of sawdust, styrofoam and high density polyethylene in the samples. Apparent porosity as high as 67% was calculated for the sample containing the high density polyethylene as pore formers confirming the potential of the kaolin deposits in forming porous bodies for industrial application. Sample with the HDPE gave the highest porosity of 67.13% while sample G showed the lowest value of 28.63%. Sample G which is the sample of batch mix containing only kaolin is seen to have less pores by virtue of the absence of porogenic materials, hence, it can be said that sample G is a non-porous sample. This assertion is in line with Guzman (2003). Also, it can be rightly observed that the higher the percentage weights of pore formers in a sample, the higher the porosity. This is for the obvious reasons of the porogen creating more voids in the sample.

4. Conclusions

The viability of producing porous ceramic bodies from West African regional kaolin deposits using various pore formers at elevated temperature (≈1150 °C) for catalytic substrate applications has been successfully explored. The XRD analysis of the samples using the Hinckley's index and Scherrer theory indicates that the Kibi kaolin which was used as a plasticizer was well ordered than the Kankara kaolin. This was morphologically confirmed from the scanning electron microscopy data. TG/DSC has been used to study the thermal behaviors of the various samples. From optical and electron microscopy studies, it was observed that after firing at 1150 °C, the as-formed uniform compact green bodies containing combustible pore formers become distorted. Samples with high density polyethylene as pore former resulted in porous bodies, confirming that the choice of pore formers is critical in

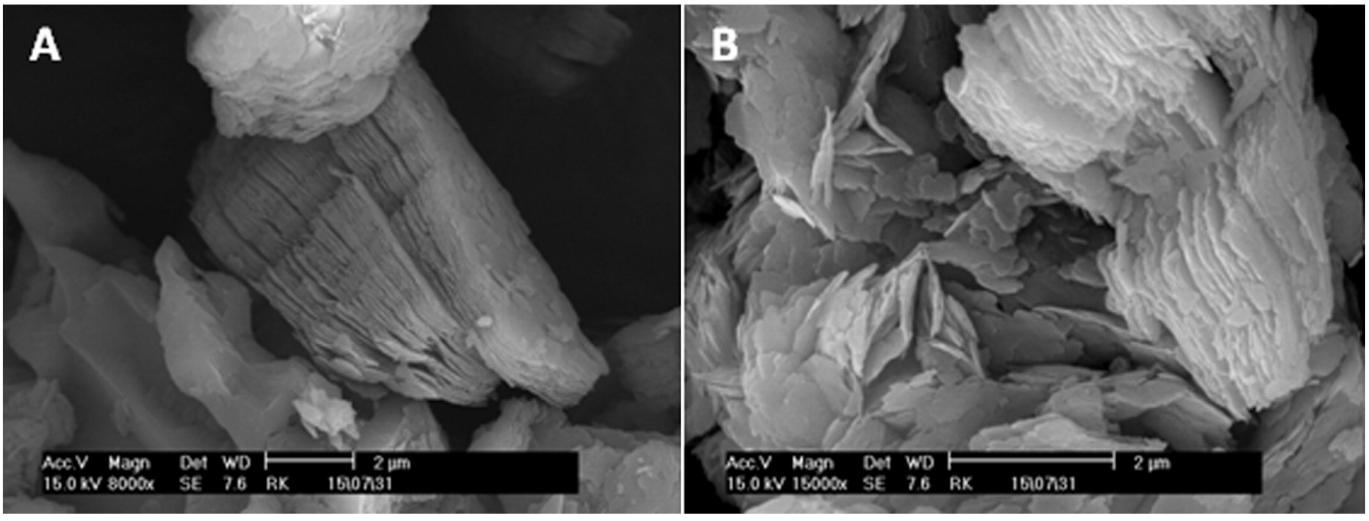

Plate I. SEM images of raw Kankara kaolin at magnifications of (A) 8000× (B) 15,000×.

Please cite this article as: Obada, D.O., et al., Potentials of fabricating porous ceramic bodies from kaolin for catalytic substrate applications, Appl. Clay Sci. (2016), http://dx.doi.org/10.1016/j.clay.2016.06.006

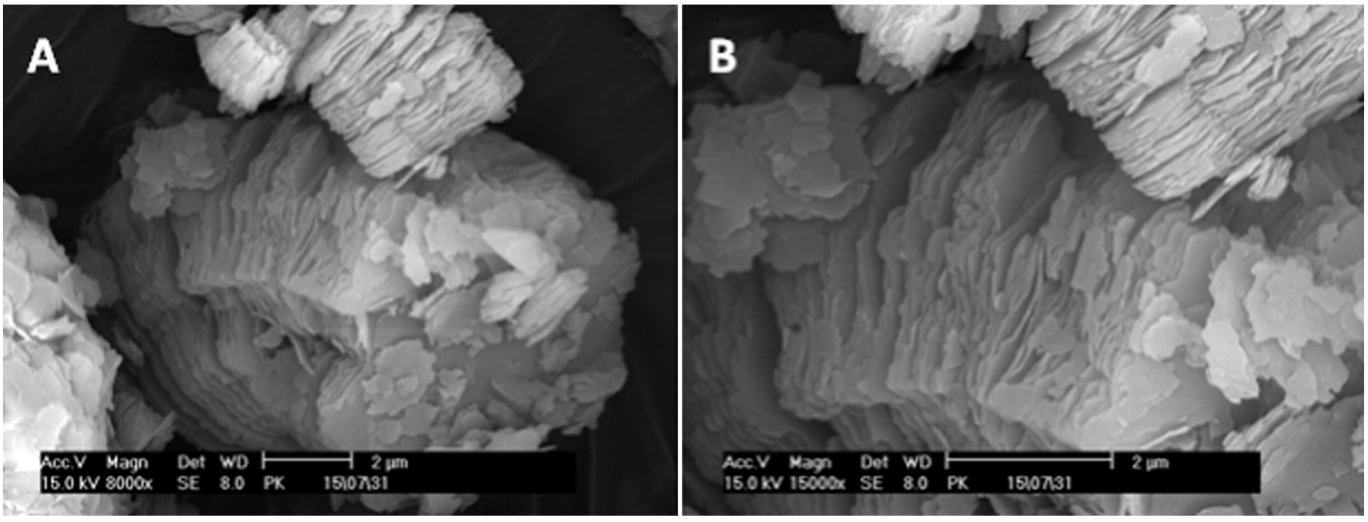

Plate II. SEM images of beneficiated Kankara kaolin at magnifications of (A) 8000× (B) 15,000×.

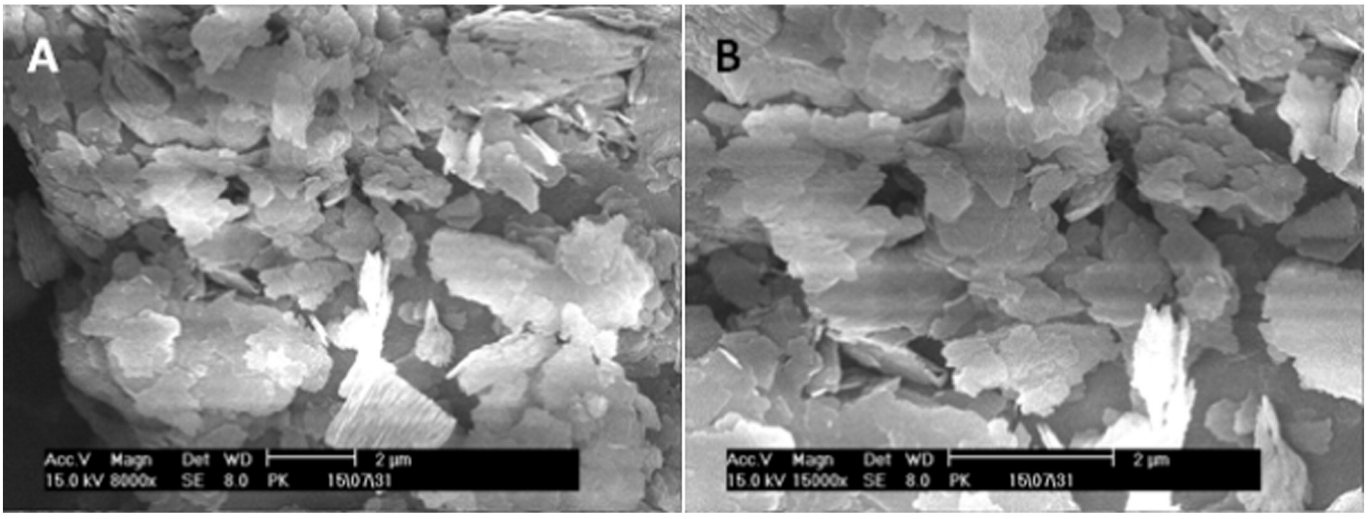

Plate III. SEM images of raw Kibi kaolin at magnifications of (A) 8000× (B) 15,000×.

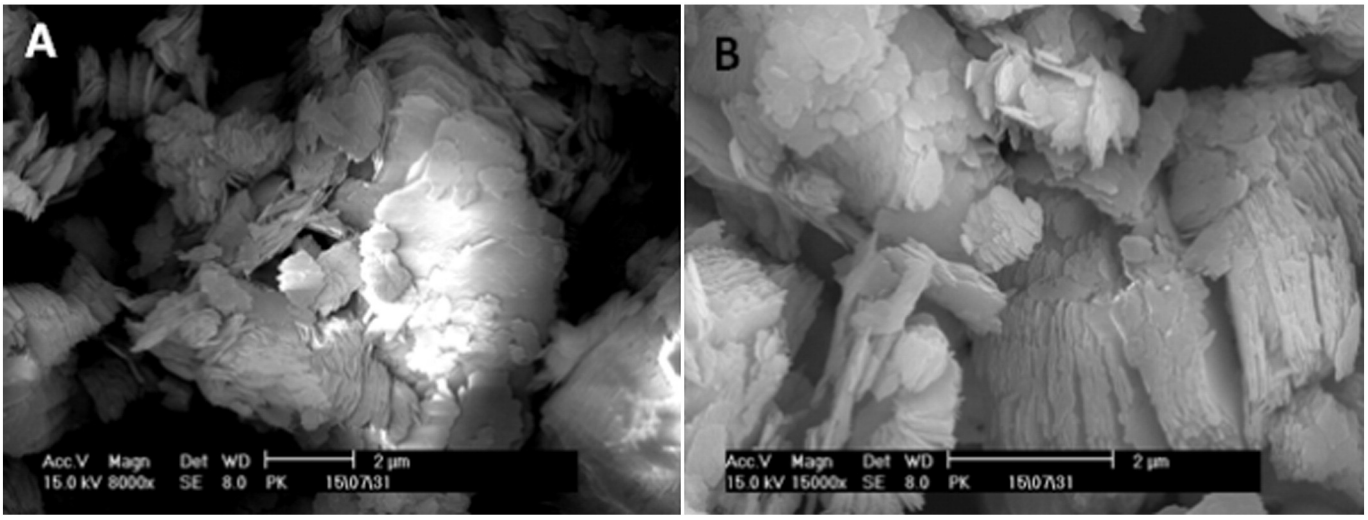

Plate IV. SEM images of beneficiated Kankara kaolin at magnifications of (A) 8000× (B) 15,000×.

Please cite this article as: Obada, D.O., et al., Potentials of fabricating porous ceramic bodies from kaolin for catalytic substrate applications, Appl. Clay Sci. (2016), http://dx.doi.org/10.1016/j.clay.2016.06.006

Table 3
Values of porosity and standard deviation for all samples.

Sample code	% P_1	% P_2	% P_3	% P_4	% P_5	% P_{avg}	SD
A	47.13	47.01	47.12	47.10	47.11	47.09	0.05
B	50.21	50.17	50.15	50.20	50.18	50.18	0.02
C	41.30	41.27	41.21	41.25	41.21	41.24	0.03
D	46.53	46.50	46.51	46.47	46.51	46.50	0.02
E	52.87	52.84	52.87	52.81	52.84	52.85	0.02
F	67.13	67.10	67.12	67.11	67.10	67.11	0.01
G	28.63	28.61	28.63	28.60	28.61	28.61	0.01

% P_{1-5} = Percentage porosities of the 5 samples for each batch formulation.
SD = Standard deviation.

achieving porous ceramic bodies. Formulations containing 80% kaolin can be used for the production of porous ceramics with porosities as high as 67% employing the appropriate pore formers for specific applications.

References

Abo-El-Enein, S.A., Heikal, M., Amin, M.S., Negm, H.H., 2013. Reactivity of dealuminated kaolin and burnt kaolin using cement kiln dust or hydrated lime as activators. Constr. Build. Mater. 47, 1451–1460.

Adams, J.M., McCabe, R.W., 2006. Clay minerals as catalysts. In: Bergaya, F., Theng, B.K.G., Lagaly, G. (Eds.), Handbook of Clay Science. Elsevier, Amnsterdam, pp. 541–581.

Al-Zahrani, A., Abdel-Majid, M.H., 2004. Production of liquid alum coagulant from local Saudi clays. J kau. Eng. Sci. 15 (1), 3–17.

Antunes, R.A., Santa, B., Michael, A., Gracher, H., Cabral, N., 2013. Geopolymer synthetized from bottom coal ash and calcined paper sludge. J. Clean. Prod. 57, 302–307.

Aparicio, P., Galán, E., 1999. Mineralogical interference on kaolinite crystallinity index measurements. Clay Clay Miner. 47, 12–27.

Aparicio, P., Galán, E., Ferrell, R.E., 2006. A new kaolinite order index based on XRD profile fitting. Clay Miner. 41 (4), 811–817.

Bai, J., Yang, X., Shi, Y., Xu, S., Yang, J., 2012. Fabrication of directional SiC porous ceramics using Fe_2O_3 as pore-forming agent. Mater. Lett. 78, 192–194.

Bergaya, F., Lagaly, G., 2013. Handbook of Clay Science. second ed. Elsevier, Amsterdam, Netherlands, pp. 18–295.

Bergaya, F., Theng, B.K.G., Lagaly, G. (Eds.), 2006. Handbook of Clay Science. Elsevier, Amnsterdam.

Bich, C., Ambroise, J., Péra, J., 2009. Influence of degree of dehydroxylation on the pozzolanic activity of metakaolin. Appl. Clay Sci. 44 (3), 194–200.

Boaro, M., Vohs, J.M., Gorte, J., 2003. Synthesis of highly porous yttria stabilized zirconia by tape-casting methods. J. Am. Ceram. Soc. 86, 395–400.

Brigatti, M.F., Galan, E., Theng, B.K.G., 2006. Structures and mineralogy of clay minerals. Handbook of Clay Science. Elsevier, Amsterdam, pp. 19–86.

Brindley, G.W., De Souza, S.P., De Souza, S.H., 1963. Mineralogical studies of kaolinite-halloysite clays. Am. Miner. 48, 897–910.

Chen, F., Huang, X., Wang, Y., Hu, Z., 1998. Investigation on foam ceramic filter to remove inclusions in revert alloy. Mater. Lett. 34 (3–6), 372–376.

Chen, F., Ma, L., Zhang, L., 2011. Pore structure control of starch processed silicon nitride porous ceramics with near-zero shrinkage. Mater. Lett. 65, 1410–1412.

Chmielová, M., Weiss, Z., 2002. Determination of structural disorder degree using an XRD profile fitting procedure: application to Czech kaolins. Appl. Clay Sci. 22, 65–74.

Churchman, G.J., Gates, W.P., Theng, B.K.G., Yuan, G., 2006. Clays and clay minerals for pollution control. In: Bergaya, F., Theng, B.K.G., Lagaly, G. (Eds.), Handbook of Clay Science. Elsevier, Amnsterdam, pp. 625–675.

Colombo, P., 2002. Ceramic foams: fabrication, properties and applications. Key Eng. Mater. 206-213, 1913–1918.

Ding, S., Zhu, S., Zeng, Y.P., Jiang, D., 2007. Gas permeability of mullite-bonded porous silicon carbide ceramics. J. Mater. Sci. 42, 7171–7175.

Dukhan, N., 2012. Metal Foams: Fundamentals and Applications. DEStech Publications, Inc.

Edomwonyi-Otu, L.C., Aderemi, B.O., Ahmed, A.S., Coville, N.J., Maaza, M., 2013. Influence of thermal treatment on Kankara kaolinite. Opticon1826 15 (5), 1–5.

Efavi, J.K., Damoah, L., Bensah, D.Y., Dodoo-Arhin, D., Tetteh, D., 2012. Development of porous ceramic bodies from kaolin deposits for industrial applications. Appl. Clay Sci. 65–66, 31–36.

Galos, K., 2011. Composition and ceramic properties of ball clays for porcelain stoneware tiles manufacture in Poland. Appl. Clay Sci. 51 (1–2), 74–85.

Garrido, L.B., Albano, M.P., Genova, L.M., Plucknett, K.P., 2011. Influence of starch type on characteristics of porous 3Y–ZrO_2 prepared from a direct consolidation casting method. Mater. Res. 14, 39–45.

Gasparini, E., Tarantino, S.C., Ghigna, P., Riccardi, M.P., Cedillo-González, E.I., Siligardi, C., Zema, M., 2013. Thermal dehydroxylation of kaolinite under isothermal conditions. Appl. Clay Sci. 80-81, 417–425.

Gregorová, E., Pabst, W., 2007. Porous ceramics prepared using poppy seed as a pore-forming agent. Ceram. Int. 33, 1385–1388.

Gregorová, E., Zivcová, Z., Pabst, W., 2006. Porosity and pore space characteristics of starch-processed porous ceramics. J. Mater. Sci. 41, 6119–6122.

Guzman, I.Y., 2003. Certain principles of formation of porous ceramic structures. Properties and applications: a review. Glas. Ceram. 60 (9–10), 280–283.

Hammel, E.C., Ighodaro, O.L.R., Okoli, O.I., 2014. Processing and properties of advanced porous ceramics: an application based review. Cer. Inter. Part A 40 (10), 15351–15370.

Hinckley, D., 1963. Variability in "crystallinity" values among the kaolin deposits of the coastal plain of Georgia and South Carolina. Clay Clay Miner. 11, 229.

Horri, B.A., Selomuya, B.P., Wang, H., 2012. Characteristics of Ni/YSZ ceramic anode prepared using carbon micropheres as a pore former. Int. J. Hydrog. Energy 37, 15311–15319.

Hosseini, S.A., Niaei, A., Salari, D., 2011. Production of γ-Al_2O_3 from Kaolin. Open J. Phys. Chem. 1, 23–27.

Khattab, R.M., Wahsh, M.M.S., Khalil, N.M., 2012. Preparation and characterization of porous alumina ceramics through starch consolidation casting technique. Ceram. Int. 38, 4723–4728.

Kim, J.K., Pal, K., 2010. Wood plastic composite foam applications: recent advances in the processing of wood-plastic composites. Eng Mater. Series 32, 165–172.

Kingery, W.D., Bowen, H.K., Uhlmann, D.R., 1976. Introduction to Ceramics. John Wiley & Sons Inc, New York, pp. 209–210.

Kumar, B.P., Kumar, H.H., Kharat, D.K., 2005. Study on pore-forming agents in processing of porous piezoceramics. J. Mater. Sci. Mater. Electron. 16, 681–686.

Li, W., Lu, K., Walz, J.Y., 2012. Fabrication of porous nanocomposites with controllable specific surface area and strength via suspension infiltration. Langmuir 27, 28 (47), 16423–16429.

Liu, Q., Tang, Z., Ou, B., Liu, L., Zhou, Z., Shen, S., Duan, Y., 2014. Design, preparation, and application of ordered porous polymer materials. Mater. Chem. Phys. 144, 213–225.

Madejová, J., Komadel, P., 2001. Baseline studies of the clay minerals source society: infrared methods. Clays Clay Miner. 49, 410–432.

Muller, J.P., Bocquier, G., 1987. Dissolution of kaolinites and accumulation of iron oxides in lateritic-ferruginous modules: mineralogical and microstructural transformations. Geoderma 37, 113–136.

Murray, H.H., 2000. Traditional and new applications for kaolins, smectite and palygorskite: a general overview. Appl. Clay Sci. 17, 207–221.

Murray, H.H., 2007. Kaolin applications. In: Murray, H.H. (Ed.), Applied Clay Mineralogy. Occurrences, Processing and Application of Kaolins, Bentonites, Palygorskite-Sepiolite, and Common Clays. Elsevier, Amsterdam, pp. 85–109.

Murray, H.H., Kogel, J.E., 2005. Engineered clay products for the paper industry. Appl. Clay Sci. 29, 199–206.

Plancon, A., Zacharie, C., 1990. An expert system for the structural characterization of kaolinite. Clay Miner. 25, 249–260.

Polakovič, J., Polakovičová, J., Sokoly, J., 1983. Interaction between kaolinite surface and hematoxyline. Proc. 5th Meeting of Eur. Clay Grp, Prague, pp. 279–282.

Prost, R., Dameme, A., Huard, E., Driard, J., Leydecker, J.P., 1989. Infrared study of structural OH in kaolinite, dickite, nacrite, and poorly crystalline kaolinite at 5 to 600 K. Clays Clay Miner. 37, 464–468.

Ray, A.M., Gautier, H., Bouler, J.M., Weiss, P., Merle, C., 2010. A new technological procedure using sucrose as porogen compound to manufacture porous biphasic calcium phosphate ceramics of appropriate micro and macrostructure. Ceram. Int. 36, 3–101.

Richerson, D.W., 2006. Modern Ceramic Engineering-Processing, Properties and Use in Design. third ed. Taylor and Francis CRC Press, New York.

Sandford, P., Sibley, S.R., 1996. Optimization of Al casting productivity using foam filter technology and application. AFS Transac. 227, 1063–1068.

Sanson, A., Pinasco, P., Roncari, E., 2008. Influence of pore formers on slurry composition and microstructure of tape cast supporting anodes for SOFCs. J. Eur. Ceram. Soc. 28, 1221–1226.

Sarikaya, S., Dogan, F., 2013. Effect of various pore formers on the microstructural development of tape-cast porous ceramics. Ceram. Int. 39, 403–413.

Scherrer, P., 1918. Nachr. Ges. Wiss. Göttingen. Mathematisch-Physikalische Klasse. 2, 98.

Seržane, R., Locs, J., Berzina-Cimdina, L., Sadretdinovs, R., 2010. Development of porous ceramics by lycopodium using uniaxial pressing and sintering. Process. Appl. Cer. 4, 231–235.

Silva, M.H.P., Lemos, A.F., Gibson, I.R., Ferreira, J.M.F., Santos, J.D., 2002. Porous glass reinforced hydroxyapatite materials produced with different organic additives. J. Non-Cryst. Solids 304, 286–292.

Studart, A.R., Gonzenbach, U.T., Tervoort, E., Gauckler, 2006. Processing routes to macroporous ceramics: a review. Am. Cer. Soc. 89, 1771–1789.

Taslicukur, Z., Balaban, C., Kuskonnaz, W., 2007. Production of ceramic foam filters from molten filtration using expanded polystyrene. J. Eur. Ceram. Soc. 27, 637–640.

Ulyanova, T.M., Krutko, N.P., Matrunchik, Y.V., Dyatlova, E.M., Paemurd, E.S., 2006. Glas. Ceram. 63, 411–414.

Please cite this article as: Obada, D.O., et al., Potentials of fabricating porous ceramic bodies from kaolin for catalytic substrate applications, Appl. Clay Sci. (2016), http://dx.doi.org/10.1016/j.clay.2016.06.006

Wang, C., Kasuga, T., Nogami, M., 2005. Macroporous calcium phosphate glass–ceramic prepared by two-step pressing technique and using sucrose as a pore former. J. Mater. Sci. Mater. Med. 16, 739–744.
Yao, X., Tan, S., Jiang, D., 2005. Improving the properties of porous hydroxyapatite ceramics by fabricating methods. J. Mater. Sci. 40, 4939–4942.
Yusiharni, E., Gilkes, R., 2012. Rehydration of heated gibbsite, kaolinite and goethite: an assessment of properties and environmental significance. Appl. Clay Sci. 64, 61–67.
Zeng, J.T., Dong, X., Chen, S.T., Yang, H., 2007. Processing and piezoelectric properties of porous PZT ceramics. Ceram. Int. 33, 395–399.
Zivcová, Z., Gregorová, E., Pabst, W., 2007. Porous alumina ceramics produced with lycopodium spores as pore-forming agents. J. Mater. Sci. 42, 8760–8764.
Zivcová, Z., Gregorová, E., Pabst, W., 2008. Alumina ceramics prepared with new pore-forming agents. Process. Appl. Cer. 2, 1–8.
Zivcová, Z., Gregorová, E., Pabst, E., 2009. Starch as a pore-forming and body forming agent in ceramic technology. Starch 61, 495–502.
Zivcová, Z., Gregorová, E., Pabst, W., 2010. Low- and high-temperature processes and mechanisms in the preparation of porous ceramics via starch consolidation casting. Starch 62, 3–10.
Zivcová, Z., Locs, J., Keuper, M., Sedlárova, I., Chmelicková, M., 2012. Microstructural comparison of porous oxide ceramics from the system Al_2– ZrO_2 prepared with starch as a pore-forming agent. J. Eur. Ceram. Soc. 32, 2163–2172.

Please cite this article as: Obada, D.O., et al., Potentials of fabricating porous ceramic bodies from kaolin for catalytic substrate applications, Appl. Clay Sci. (2016), http://dx.doi.org/10.1016/j.clay.2016.06.006